

Coherent cross-talk and parametric driving of matter-wave vortices

N. G. Parker,* A. J. Allen, C. F. Barenghi, and N. P. Proukakis

School of Mathematics and Statistics, Newcastle University, Newcastle upon Tyne, NE1 7RU, UK

(Dated: September 2, 2011)

We show that the interaction between vortices and sound waves in atomic Bose-Einstein condensates can be elucidated in a double-well trap: with one vortex in each well, the sound emitted by each precessing vortex can be driven into the opposing vortex (if of the same polarity). This cross-talk leads to a periodic exchange of energy between the vortices which is long-range and highly efficient. The increase in vortex energy (obtained by numerical simulations of the Gross-Pitaevskii equation) is significant and experimentally observable as a migration of the vortex to higher density over just a few precession periods. Similar effects can be controllably engineered by introducing a precessing localised obstacle into one well as an artificial generator of sound, thereby demonstrating the parametric driving of energy into a vortex.

PACS numbers: 03.75.Kk, 03.75.Lm

I. INTRODUCTION

In a quantum fluid, such as an atomic Bose-Einstein condensate (BEC) or superfluid Helium, vortices possess quantized circulation, synonymous with them being a topological defect in the macroscopic condensate phase. Quantized vortex lines, rings, lattices and tangles have been the subject of experimental study in superfluid Helium for over 50 years [1], and in which recent emphasis has been on their role in quantum turbulence [2, 3]. Meanwhile, since the late 1990's, there has been fast-growing interest in vortices in Bose-Einstein condensates [4, 5], where the controllability of these gases has led to the generation of single vortices [6, 7], giant vortices [8], vortex dipoles [9], soliton-vortex hybrids [10] and turbulent vortex tangles [11]. It is worthy of note that recent breakthroughs in imaging of both Helium [12] and BEC [13] systems now enable the dynamics of quantized vortices to be monitored in real-time.

The full nature of the vortex-sound interaction in quantum fluids is unclear [14]. The superfluid topology constrains quantized vortices to disappear by annihilating with an oppositely charged vortex or vanishing at the edge of the system (where they annihilate with their image). In the limit of zero temperature and for a uniform condensate, sound waves are the low-lying excitations of the system and provide the only energy sink for vortex decay. For example, at zero temperature the reconnection of vortex lines [15] and the acceleration of a vortex line segment both generate sound waves [16, 17], dissipating the vortical energy. In the latter case, the acceleration that drives sound emission may arise from the influence of other vortices [18, 19], Kelvin waves excitations of vortex lines [20] or the Magnus force in an inhomogeneous ambient density, e.g. in a trapped condensate [21]. The experimentally observed decay of vorticity at very low temperature in superfluid He [22, 23] is thought to be

primarily due to the Kelvin waves dissipation route, with reconnections playing a secondary role [3].

Less well understood is the inverse process, i.e. the absorption of sound by a vortex. Insight may be gleaned from vortex-sound interactions in fluid dynamics [14]. For example, an acoustic ray model has predicted that certain trajectories of sound wave can spiral into the vortex core, transferring energy to the vortical flow [24, 25]. While sound waves can induce the nucleation of vortices through the collapse of cavitating bubbles [26, 27], sound absorption by pre-existing vortices is not thought to play a significant role in homogeneous superfluid Helium systems. However, sound absorption may become considerable in atomic BECs due to their confined geometry. Indeed, the lack of sound-induced decay of a vortex precessing in a harmonically-trapped BEC has been attributed to reabsorption of the emitted sound [21] (although related works [4, 16] predict that the sound emission may be prohibited due to the sound wavelength exceeding the system size). The harmonic nature of the trap appears key to supporting a sound-vortex equilibrium, with trap anharmonicities apparently leading to net vortex decay [21, 28], in analogy to dark solitons [29, 30]. However, it is difficult to resolve the interaction of sound and vortices in single trapped condensates [19, 21] due to their co-habitation in the trap.

Analogous questions exist over the interaction of matter-wave dark solitons with sound. Like vortices, they radiate sound waves under acceleration [29, 31], become stabilised in harmonic traps [21] and can be parametrically driven by artificially generated sound waves [18]. Recently, a double-well trap was shown to offer beneficial insight into the soliton-sound interaction [32]. With one soliton in each well, large-scale exchanges in energy between the solitons clearly demonstrated a long-range sound-mediated interaction.

Here we will exploit a double well trap to study the emission and absorption of sound by vortices. We will begin by considering an idealized double trap geometry. The trap system and theoretical model are outlined in Section II. In Section III we consider how a single vortex

*Electronic address: nick.parker@ncl.ac.uk

behaves in this system (while not the main results of our work, this an essential prerequisite to understanding the dynamics in later sections). In Section IV we progress to consider how two vortices, one in each well, interact via the exchange of sound waves or “cross-talk”. In Section V we replace one of the vortices with a moving obstacle, and explore how the sound generated interacts with the remaining vortex. In Section VI we discuss our theoretical findings. In Section VII we demonstrate the same qualitative behaviour in an experimentally-achievable double trap geometry. Finally, in Section VIII we draw conclusions of our work.

II. THEORETICAL FRAMEWORK AND TRAP SET-UP

We consider a BEC at ultracold temperatures such that thermal and quantum fluctuations can be neglected and that the system is well parameterised by a mean-field order parameter $\Psi(\mathbf{r}, t)$ which satisfies the three-dimensional Gross-Pitaevskii equation (GPE) [33]. We assume a quasi-2D geometry, whereby harmonic trapping is sufficiently tight in one dimension, taken here to be the z -direction, to freeze out the corresponding dynamics. Then, using the decomposition $\Psi(\mathbf{r}, t) = \psi(x, y, t)\psi_z(z)$, one can integrate out the time-independent axial component $\psi_z(z)$ from the 3D GPE. The transverse order parameter $\psi(x, y, t)$ then satisfies the 2D GPE,

$$i\hbar\partial_t\psi = \left(-\frac{\hbar^2}{2m}\nabla^2 + V(x, y) + g|\psi|^2 - \mu\right)\psi, \quad (1)$$

where $V(x, y)$ is the axial trapping potential and m is the atomic mass. The 2D chemical potential μ is related to the 3D chemical potential μ' via $\mu = \mu' - \hbar\omega_z/2$, where ω_z is the trap frequency in the axial direction. s -wave atomic interactions, of length a , give rise to the nonlinear term with coefficient $g = 2\sqrt{2\pi}\hbar^2 a/ml_z$, where $l_z = \sqrt{\hbar/m\omega_z}$ is the harmonic oscillator length of the frozen dimension.

The complex order parameter $\psi(x, y, t)$ can be written as $\psi(x, y, t) = \sqrt{n(x, y, t)}\exp[i\phi(x, y, t)]$, where $n(x, y, t)$ and $\phi(x, y, t)$ are the distributions of atomic density and phase, respectively. Furthermore, the phase defines the fluid velocity $\mathbf{v} = (\hbar/m)\nabla\phi$. In 2D vortices are singular points about which the phase wraps around by an integer multiple of 2π and the condensate flows azimuthally. The density is pinned to zero at the central point creating a well-defined vortex core which relaxes to its unperturbed value at a distance of the order of the healing length $\xi = \hbar/\sqrt{mn_0g}$.

We will initially consider an idealized double well system consisting of two connected harmonic traps,

$$V(x, y) = \frac{1}{2}m\omega^2 \left[(|x| - x_c)^2 + y^2 \right]. \quad (2)$$

Each trap is circularly symmetric with frequency ω and displaced from the origin by $\pm x_c$, as illustrated in Fig.

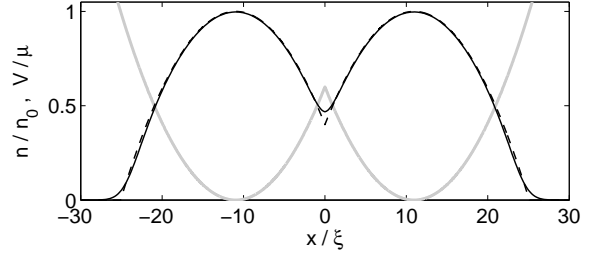


FIG. 1: Vortex-free density profile at $y = 0$ along the x -axis (black solid line) in the double harmonic potential (grey solid line) with a barrier height at $x = 0$ of $V_0 = 0.6\mu$. The corresponding Thomas-Fermi profile $n_{\text{TF}} = (\mu - V)/g$ is also shown (black dashed line).

1. The barrier separating the trap, which has a minimum height of $V_0 = \frac{1}{2}m\omega^2 x_c^2$, determines the connectivity between the wells and thus the degree to which sound and vortices can propagate between wells. The transfer of sound waves, which have energy of order μ , between the wells will be possible for $V_0 < \mu$ and prohibited for $V_0 \gg \mu$. The capacity for vortices to propagate between wells will depend additionally on the energy of the vortex.

While this trap is not directly achievable in experiments due to its sharp feature at $x = 0$, it is convenient to consider theoretically: it identifies the main physical effect in a “clean” manner and allows us to draw on the established knowledge for vortices in harmonic traps. We will later demonstrate that the same dynamics persist in experimentally-achievable set-ups.

The 2D GPE is solved numerically using the Crank-Nicholson method [34]. Over a typical simulation, the relative change in norm and energy $\Delta N/N$ and $\Delta E/E$ are of order 10^{-6} , i.e. the solution is numerically well converged. The vortex-free ground state, with density profile $n_{\text{VF}}(x, y)$, is found by propagating the 2D GPE in imaginary time. Vortical states are imposed by forcing the phase distribution (during imaginary time propagation) to,

$$\phi(x, y) = \prod_i q_i \arctan \left(\frac{y - y_i}{x - x_i} \right), \quad (3)$$

where i is the index of a vortex with charge q_i located at (x_i, y_i) . Since multiply-charged vortices are energetically unfavourable compared to multiple singly-charged vortices [1, 33], we shall only consider singly-charged vortices $|q_i| = 1$ (relative polarity may change). We will infer the change in energy of vortices in our system through changes in their position, e.g. a drift to lower density signifies a decrease in the vortex energy. This is exactly what would be done in reality, since the vortex energy cannot be directly measured experimentally.

We assume units in which length, speed and energy are expressed in terms of the 2D healing length $\xi = \hbar/\sqrt{mn_0g}$, speed of sound $c = \sqrt{n_0g/m}$ and chemical potential $\mu = n_0g$, where n_0 is the peak density.

The ratio $\mu/\hbar\omega$ specifies the nature of the condensate. For $\mu/\hbar\omega \ll 1$ the trap dominates and the ground state will approximate the gaussian harmonic oscillator. For $\mu/\hbar\omega \gg 1$ the interactions dominate and lead to a broad condensate profile. Then the kinetic energy of the ground state, which depends on the gradient of the density, becomes negligibly small. Under this Thomas-Fermi (TF) approximation, the density takes the analytic form $n_{\text{TF}} = (\mu - V)/g$ [33].

We focus on a system with $\mu/\hbar\omega = 10$. An example density profile is shown in Fig. 1. It is closely matched by the TF prediction, with the only significant deviation arising at the condensate perimeter and the barrier. There the density gradient is not negligible, resulting in a smoothening of the density over a lengthscale $\sim \xi$. The TF approximation predicts a condensate radius $R_{\text{TF}} = \sqrt{2\mu/m\omega^2} = 14.14\xi$. While we hereafter express length in terms of healing length, this can be trivially related to the trap harmonic oscillator length $l_{\text{ho}} = \sqrt{\hbar/m\omega}$ via $l_{\text{ho}} = \sqrt{10}\xi$.

III. SINGLE VORTEX

We first explore the dynamics of a single vortex within the double trap system (2). A vortex tends to follow a path of equipotential through a trapped condensate, e.g., precessing around the trap centre in a single harmonic trap [35]. In the double trap we can additionally anticipate a regime in which the vortex can follow a dumbbell-shaped path around both wells. As is well known for single harmonic traps, the energy and angular momentum associated with the vortex increases as the vortex is moved to higher density, i.e. towards the centre of the well [4, 33].

We place a vortex in the right-hand well at a position $(x_c, y_c + r_v)$, where $(x_c, y_c) = ([2V_0/m\omega^2]^{1/2}, 0)$ is the origin of the right-hand trap and r_v is the initial offset of the vortex from the well centre. NB the dynamics are insensitive to the direction of the off-set. The ensuing dynamics are sensitive to the size of the vortex displacement r_v and the inter-trap barrier V_0 . We numerically evolve the vortex dynamics over a long simulation time ($5000 (\xi/c)$) within this parameter space. Note when the vortex is initially positioned very close to BEC edge (typically within one healing length of R_{TF}) its evolution is indistinguishable from surface excitations that are generated. This is a general consequence of being initiated in the low density periphery and occurs even in isolated harmonic traps. As such we do not present the vortex dynamics at such extreme positions.

The phase diagram for the vortex dynamics is plotted in Fig. 2, separating regions of ‘stable’ vortex dynamics (dots) from those where there is no vortex within the system in the ‘final’ simulated state (crosses), as discussed in detail below. Note that we observe a qualitatively similar phase diagram for a larger (more TF-like) condensate.

A. Stable dynamics

If dissipationless, we would expect the vortex to always remain in the system. In Fig. 2 we see regimes where this is true (dots) but also where the vortex is unstable and ultimately leaves the system (crosses). Stable vortex motion is promoted for large V_0 , since the well then behaves like an isolated harmonic trap, and for low vortex radii, since the vortex does not feel a strong effect from the far trap. Under this stable motion the vortex dynamics is akin to that in a single harmonic trap [36]: it precesses around the well centre with approximately constant radius and generates a collective motion of the background condensate of low amplitude ($\sim 5\%n_0$). In Fig. 3 we show a typical snapshot of the condensate. The density distribution consists of two weakly-connected circular condensates and the vortex appears as a hole (white spot) in the right-hand well. By subtracting the time-independent vortex-free density n_{VF} from this density profile, the collective excitation become clearly visible (Fig. 3). The precession frequency of the vortex is $\sim 0.2\omega$ for small displacements, and increases with r_v , in good agreement with analytic predictions for vortex precession in a single harmonic trap in the TF regime [37].

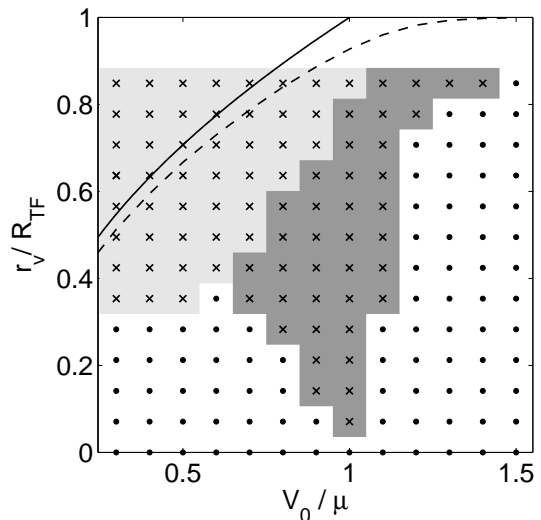


FIG. 2: Phase diagram in $r_v - V_0$ space for the single vortex case showing whether the final state of the system (after a long simulation time of $5 \times 10^3 (\xi/c)$) is a single vortex (dots) or the vortex-free state (crosses). The light-shaded region is the cross-over regime (case I), in which the vortex passes into the far well. The dark-shaded region is the inductive regime (case II), in which the initial vortex induces other vortices. The lines are the TF predictions for the onset of cross-over dynamics $r_v/R_{\text{TF}} = \sqrt{(1 - n_{\text{min}}/n_0)}$ using the TF prediction (solid line) and the numerical values (dashed line) for n_{min} . The observed deviation between these lines and the light/dark grey boundary acts as an indication of the importance of sound emission in the actual vortex dynamics. The TF radius of each well is $R_{\text{TF}} = 14.14\xi$.



FIG. 3: (Left) Density $n(x, y)$ for the single vortex scenario with $y_v = 1\xi$ and $V_0 = 0.9\mu$ at a time of $1000 \xi/c$. Black (white) corresponds to peak (zero) density. (Right) Renormalised density $n(x, y) - n_{VF}(x, y)$ for the same data as above. The colorscale is $\pm 10\% n_0$. Each box is of size $64\xi \times 32\xi$.

B. Unstable dynamics

In cases where the vortex eventually decays from the system (crosses in Fig. 2) its initial dynamics falls into one of two cases. In case I, the dynamics is characterised by the vortex *crossing over* into the adjacent well, whereas in case II it is characterised by *inducing* a mirror vortex in the adjacent well. These effects most commonly become manifested in the first precession of the vortex in the trap, but in a minority of cases they may arise after several precessions.

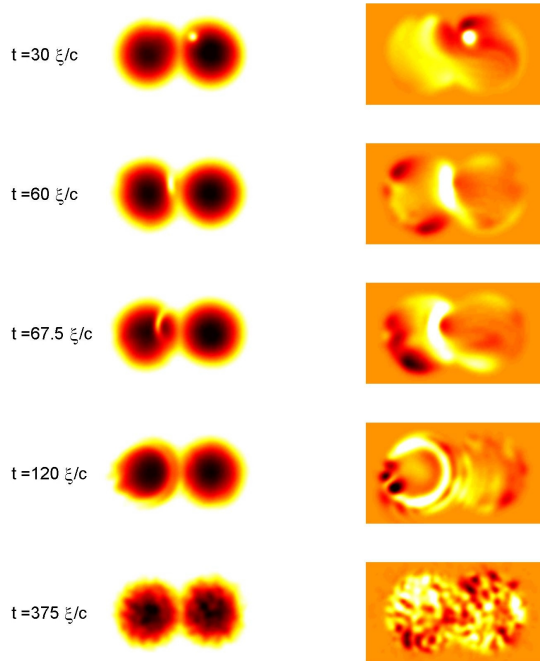


FIG. 4: Crossover regime dynamics: Snapshots of (left) density $n(x, y)$ and (right) renormalized density $n(x, y) - n_{VF}(x, y)$ within the crossover regime, for $r_v = 8\xi$ and $V_0 = 0.6\mu$, at various times. (Spatial and color scales are the same as in Fig. 3).

1. Case I: vortex crossover

Case I (vortex crossover) arises in the lightly shaded region in Fig. 2. The vortex can be expected to travel between the wells when the local potential of the vortex (the value of the potential at the vortex core) exceeds the inter-well barrier. This will tend to occur for large vortex off-sets and a weak inter-trap barrier. Put quantitatively, one would expect cross-over to occur when the vortex density depth n_v is less than or equal to the minimum density at the barrier n_{\min} (one can picture this as when the vortex can just squeeze through the barrier). If dissipationless, the density depth of the vortex will retain its initial value, which we can approximate via the TF prediction $n_v = n_0(1 - r_v^2/R^2)$. This is a robust approximation provided that the vortex position is away from the edge and the barrier, for which the TF density agrees with the actual density profile to within $0.01n_0$. This gives the criteria $r_v/R \geq \sqrt{1 - n_{\min}/n_0}$ for cross-over to be possible. We can first approximate n_{\min} via its TF prediction $n_{\min}^{\text{TF}} = n_0(1 - V_0/\mu)$, giving the solid line. However, the onset of cross-over dynamics occurs at considerably lower r_v . We can expect some deviation to arise from the inaccuracy of using the TF approximation for n_{\min} : the TF approximation underestimates the density at the point of the barrier, as evident in Fig. 1.

If we instead use the actual value of the ground-state density at the barrier, we obtain the threshold shown by the dashed line in Fig. 2. This lowers the prediction for r_v , but only slightly and the prediction still remains considerably greater than the observed threshold. This anomaly is likely to arise from the radiation sound from the vortex. This will have two implications for promoting cross-over dynamics. Firstly the dissipating vortex will move to lower densities/greater radial position. Secondly, the emitted sound generates collective modes of the BEC which will cause the density at the barrier to become time-dependent and may promote vortex cross-over during “high tide”.

In this crossover regime, the ultimate fate of the vortex is to decay. In Fig. 4 we present an example. The precessing vortex approaches the barrier ($t = 30(\xi/c)$) and upon traversing it ($t = 60(\xi/c)$), decays into a high-amplitude curved pulse of sound ($t = 67.5(\xi/c)$). The sound pulse reflects off the far left-side of the trap and propagates back through the trap ($t = 120(\xi/c)$). Following many reflections and diffractions in the trap, the sound pulse becomes randomised, ultimately forming an isotropic sound field ($t = 375(\xi/c)$).

In other cases, the vortex undergoes a more gradual decay, passing many times between the wells. NB more generally, we can observe some cases where the vortex undergoes stable cross-over dynamics, as we will see later in Section VII.

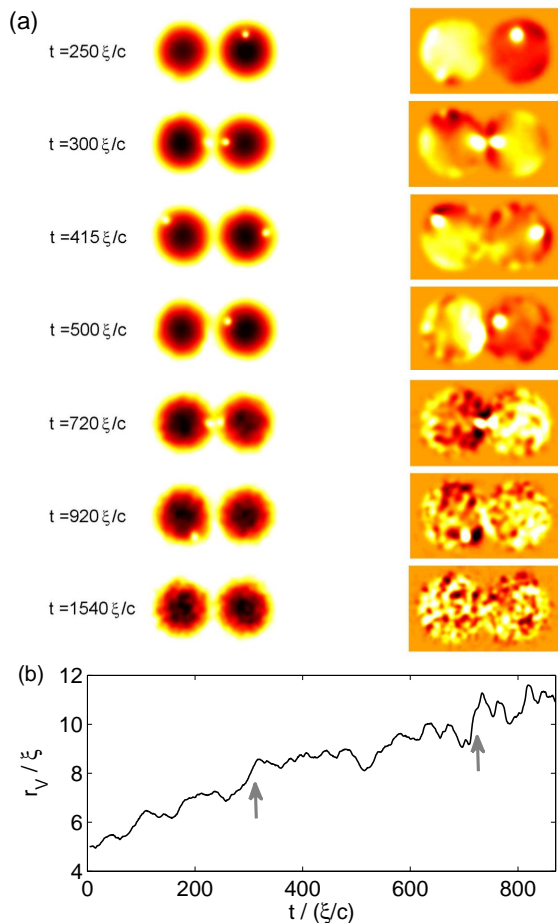


FIG. 5: Inductive regime dynamics: (a) Density $n(x,y)$ (left column) and renormalised density $n(x,y) - n_{VF}(x,y)$ (right column) at various times. Parameters: $r_v = 5\xi$ and $V_0 = 0.9\mu$ (box size and colorscale are the same as in Fig. 3). (b) Evolution of the radial position of the vortex r_v ; arrows indicate the points at which vortex induction takes place.

2. Case II: vortex induction

The second case of unstable dynamics (case II: vortex induction), characterised by the initial vortex inducing a second vortex in the far-well, arises in the dark shaded region in Fig. 2. Snapshots of a typical evolution are shown in Fig. 5. As the vortex precesses close to the adjoining well ($t = 300\xi/c$), a mirror vortex becomes excited on the opposite side of the inter-well barrier. This vortex has the opposite charge to the original vortex and precesses in the opposite direction around its trap ($t = 415\xi/c$). This early induction is the characteristic of this regime of dynamics. The subsequent dynamics can vary widely. In the example, the initially-induced vortex disappears ($t = 500\xi/c$), a second vortex is induced ($t = 720\xi/c$) and then the original right-hand vortex disappears ($t = 920\xi/c$). In other cases the original vortex may disappear as it creates its mirror vortex, while sometimes the induced vortex may itself induce a

vortex in the right-hand well. As a result there can arise periods of time where multiple vortices can appear in the system. For all cases we observe the growth of a tempestuous sound field during the vortex motion, set up by the sound emission from the accelerating vortices. All of the vortices ultimately dissipate and disappear into an energetic and isotropic sound field (Fig. 5(b) at $t = 1540\xi/c$).

Up until the point when it disappears, the original vortex drifts outwards, as shown in Fig. 5(b). Most of the noise in $r_v(t)$ is due to the buffeting effect that the sound field has on the vortex. However, the sizeable jumps in r_v at $t \sim 300$ and 700 (ξ/c) (highlighted by arrows) occur as a vortex is induced in the far well, indicating the transfer of energy from the original vortex to create the new one.

This region of the parameter space occurs for a range of barrier heights in the vicinity of $V_0 = \mu$, for which the condensate channel is of low density. The energy to create a vortex depends on the local density. As the barrier height is reduced below μ , the density in the barrier region increases and we have confirmed with numerical simulations that the energy cost to create a vortex here increases sharply.

IV. CROSS-TALK OF TWO VORTICES

We now extend to the case where there is initially a vortex in *each* well to examine the possibility of sound-induced interaction between vortices. We continue to employ the idealized double harmonic trap geometry; we will demonstrate the same phenomena in a realizable double trap geometry in Section VII. The additional vortex (denoted “vortex 2”) is created at the centre of the left-hand trap. Since it feels the velocity field of vortex 1 it will not be perfectly stationary. The displacement

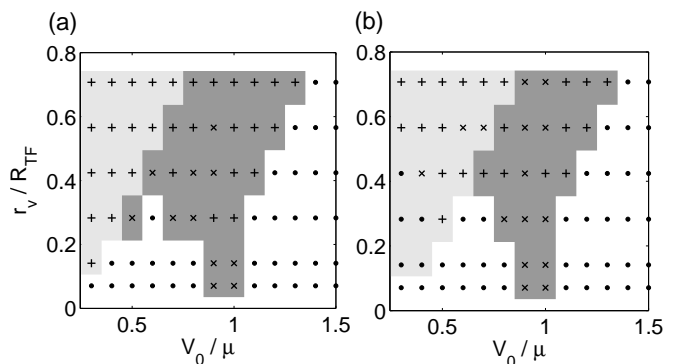


FIG. 6: Phase diagram in $r_v - V_0$ of the final state (after $5000(\xi/c)$) of the two vortex system for (a) same polarity and (b) opposite polarity of the vortices. The final state is either two stable vortices (dots), one stable vortex (pluses) or no vortices (crosses). The second vortex is initially positioned at the centre of the left-hand well. Light and dark shading indicates case I (crossover) and case II (induction) of the unstable dynamics.

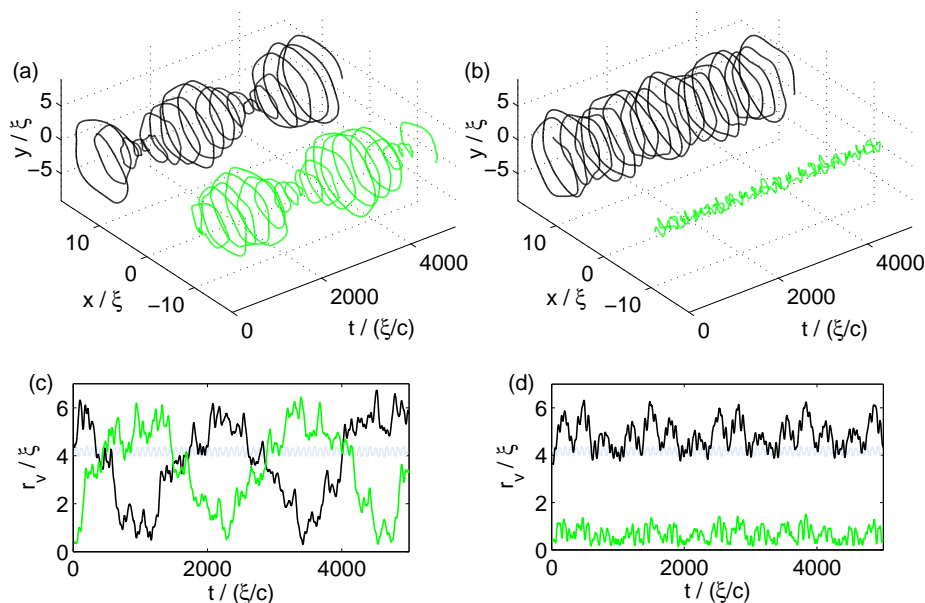


FIG. 7: Vortex dynamics in the two-vortex system with (a) the same polarity and (b) different polarity. Parameters: $r_1(t=0) = 4\xi$, $V_0 = 0.6\mu$. Black (green/dark grey) lines correspond to vortex 1 (2). (c) and (d) plot the corresponding vortex radii, and additionally include the evolution of a single vortex in an isolated harmonic trap (light blue/grey line) with initial radius $r_v(t=0) = 4\xi$.

of vortex 1, denoted r_v , and the height of the inter-well barrier, V_0 , are again key to the dynamics. The latter parameter now additionally controls the transfer of sound between the wells, since sound waves have an energy of around μ . We can also expect sensitivity to the relative polarity of the vortices. Figure 6 shows the phase diagram of the system for (a) vortices of the same polarity and (b) vortices of opposite polarity.

The phase diagrams are similar to the single vortex case (Fig. 2) and the vortex polarity only has a small effect on the final state of the system. There are two stable regions, one for weak barriers and low displacements, and the other for large barriers. We also see a cross-over regime for weak barriers and large vortex displacements in which vortex 1 tends to cross into the other well, and an induction regime for barrier heights centered around μ in which vortex 1 induces another vortex in the opposite well. Where vortex instability does occur, the end state is either the persistence of a single vortex or no vortices at all. We cannot make any general comments about what favours these two end states: the dynamics that can develop are sufficiently complex that the end state is not readily deterministic.

Note that in Fig. 6(b) there exists stable dynamics in the cross-over regime. In this case vortex 1 perpetually traverses both wells in a stable manner while vortex 2 remains localised in the centre of its well.

In order to investigate the cross-talk between vortices, that is their sound-mediated interactions, we focus on the stable regimes and in particular the stable area occurring for low barrier heights, for which one can expect unimpeded motion of sound between the wells. Figure 7

present the vortex dynamics for $r_v = 4\xi$ and $V_0 = 0.6\mu$. When the vortices have the same charge (Fig. 7(a)) the vortices periodically spiral inwards and outwards, and remain out of phase with each other. The change in vortex radial position (Fig. 7(c)) is large (the vortices oscillate between the trap centre and a radius of around $6\xi = 0.43R_{\text{TF}}$), demonstrating a significant transfer of energy between the vortices. The energy exchange occurs over a timescale of $\sim 2000(\xi/c)$, which is around 8 precessions of the vortex in the trap (the precession period is $\sim 270(\xi/c)$). In the analogous situation for the dark soliton, the energy transfer is much slower, occurring over many tens of soliton oscillations [32]. The periodic change in vortex radius (Fig. 7(c)) is composed of sharp steps, suggesting that the energy emission and absorption of the vortices occurs in packets rather than continuous.

In Fig. 7(c) we also present, for comparison, the evolution of a single vortex in an isolated harmonic trap (light blue/grey line). The vortex maintains an approximately constant radius, with only small-scale modulations due to its re-interaction with its emitted sound and collective modes [36].

When the vortices have opposing polarity (Fig. 7(b) and (d)), no significant transfer of energy is observed and the vortices precess with approximately constant radius. The vortex motion does undergo modulations but these are not out-of-phase and so do not constitute a direct exchange of energy. Rather the modulations arise from the back-action of the randomised sound field on the vortices. These modulations are larger than the corresponding ones experienced by a single vortex in a har-

monic trap, indicative of the greater sound density in the double well system.

The significant transfer of energy between like-charged vortices and insignificant transfer between unlike-charged vortices is consistent across the stable region of the parameter space at low barrier heights. In the region of stable dynamics at high V_0 we do not observe a significant transfer in energy between the vortices since the transfer of sound across the barrier becomes prohibited.

It would appear that the vortices periodically drive energy into each other via their emitted sound. However, we must rule out that this effect arises from the long-range interaction between vortices due to their superimposed velocity fields. To this aim, we will next attempt to drive a vortex via sound waves generated by artificial means - a moving localised barrier.

V. PRECESSING OBSTACLE

We now replace the left-hand vortex with a precessing obstacle. Note that we continue to employ the idealized double harmonic trap; the same effects will be demonstrated in an experimentally realizable trap in Section VII. The obstacle corresponds to a time-dependent potential,

$$V_{\text{ob}}(x, y, t) = A_{\text{ob}} \times \exp \left[-\frac{\{x + x_c - x_{\text{ob}}(t)\}^2 + \{y - y_{\text{ob}}(t)\}^2}{\sigma^2} \right], \quad (4)$$

where,

$$x_{\text{ob}}(t) = \pm r_{\text{ob}} \sin(\omega_{\text{ob}} t + \phi_{\text{ob}}) \\ y_{\text{ob}}(t) = r_{\text{ob}} \cos(\omega_{\text{ob}} t + \phi_{\text{ob}}).$$

This represents a Gaussian-shaped barrier, of amplitude A_{ob} and width σ , moving in a circular path around the centre of the left-hand well with radius $r_{\text{ob}} = x_{\text{ob}}^2 + y_{\text{ob}}^2$. Such an obstacle can be induced experimentally via a blue-detuned laser beam [9, 38]. For the “-” (“+”) case above, the barrier moves in the same (opposite) direction as the vortex. ϕ_{ob} represents the relative phase between the initial position of the obstacle and the vortex (e.g. for $\phi_{\text{ob}} = 0$ the obstacle and vortex start at mirror-opposite positions in their wells).

We attempt to generate sound that mimics the sound generated by a vortex and will thus employ precession frequencies similar to those of a vortex ($\sim 0.23\omega$ for our system). This is sufficiently low to prevent the obstacle exceeding the superfluid critical velocity and nucleating vortices [9, 38–40]. We have confirmed via numerical simulations of the precessing obstacle (with no vortices imposed) that its only effect is to generate spiral sound waves with typical amplitude $\sim 1\%n_0$.

We mimic the system parameters employed in Fig. 7 [$r_v = 4\xi$ and $V_0 = 0.6\mu$] and additionally employ an obstacle potential defined by width $\sigma = 2\xi$, amplitude

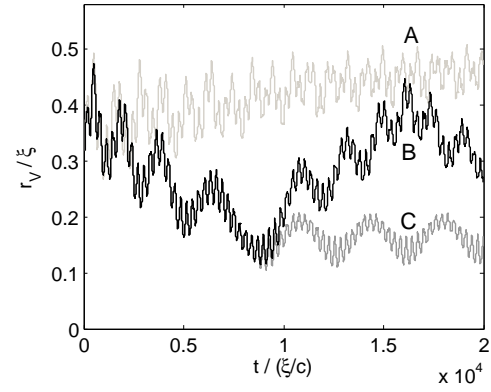


FIG. 8: Evolution of the vortex radius under the influence of a driving obstacle. Black line (B): the obstacle moves in the same direction as the vortex. Light grey line (A): the obstacle moves in the opposite direction to the vortex. Dark grey line (C): the barrier moves in the same direction as the vortex but its motion is terminated at $t=8800(\xi/c)$. Parameters: $r_1(t=0) = 4\xi$, $\sigma = 2\xi$, $r_{\text{ob}} = 4\xi$, $\phi_{\text{ob}} = 0$ and $\omega_{\text{ob}} = 0.234\omega$ and $V_0 = 0.6\mu$.

$A_{\text{ob}} = \mu$, phase $\phi_{\text{ob}} = 0$, path radius $r_{\text{ob}} = 4\xi$ and frequency $\omega_{\text{ob}} = 0.234\omega$ (these parameters are chosen as they optimise the energy transfer, as shown below). First consider the case when the barrier moves in the same direction as the vortex (solid black line in Fig. 8). We clearly see that the vortex radial position oscillates in time, i.e., there is periodic driving of energy into the vortex. This is analogous to the predicted parametric driving of a matter-wave dark soliton [18]. The energy transfer due to the obstacle is more gradual than that induced by another vortex (i.e., compare to Fig. 7), with the exchange occurring over a time of $\sim 12000 (\xi/c)$ or ~ 40 precessions. Conversely, if the barrier moves in the opposite direction to the vortex (solid green/grey line) no driving is observed (although a small outward shift of the vortex suggests a small loss of energy in this case). This is qualitatively the same behaviour as we observed earlier when the obstacle is replaced by another vortex. However, the timescale of the energy transfer is considerably slower than with the obstacle. This shows that the vortex is a much more efficient source of sound to drive another vortex.

Returning to the case where the obstacle moves in the same direction as the vortex, we find that if the obstacle motion is terminated (becoming a stationary obstacle) when the vortex is at its minimum radial position (dotted black line in Fig. 8), it maintains this minimal radial position (subject to some oscillations about this radius). In this manner we can parametrically drive net energy into the vortex. Indeed, if we terminate the obstacle motion at any point the vortex approximately maintains that radial position.

The minimum radius achieved r_{min} provides a measure of the maximal amount of energy driven into the vortex. In Fig. 9 we show how this quantity varies as a function

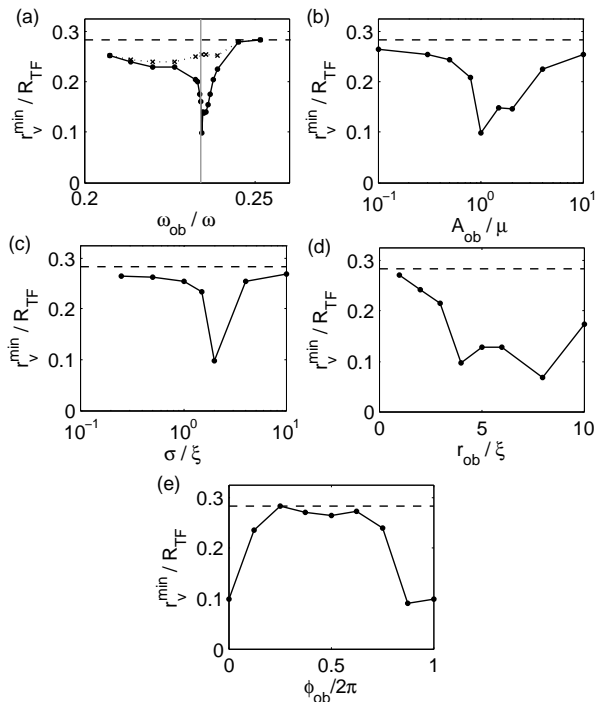


FIG. 9: Minimum radial position achieved by the vortex under the influence of a precessing Gaussian barrier during a total simulation time of $2 \times 10^4 (\xi/c)$. The vortex is initially at $r_v = 4\xi$ and the inter-well barrier height is $V_0 = 0.6\mu$. The obstacle parameters are based around the values $\omega_{ob} = 0.234\omega$, $A_{ob} = \mu$, $\sigma = 2\xi$, $r_{ob} = 4\xi$ and ϕ_{ob} , and each is varied in turn from plot (a)-(e). In (a), we present results for co-rotating (solid line with dots) and anti-rotating (dashed line with crosses) system. In (b)-(e) we consider only the co-rotating system. In each plot the initial vortex radial position is shown (dashed horizontal line). In (a) we show the precession frequency of the undriven vortex (grey vertical line).

of the obstacle parameters $\omega_{ob}, V_{ob}, r_{ob}, \sigma$ and ϕ_{ob} . For each case we observe a clear resonance that minimises r_{min} and maximises the energy that can be driven into the vortex:

- ω_{ob} [Fig. 9(a)]: When the obstacle direction is the same as the vortex (black line/dots) we see a clear frequency resonance, with maximal energy being driven into the vortex for a precession frequency close to that of the undriven vortex (vertical dotted line). For the opposite case, the minimum radius achieved undergoes no significant resonance. For this reason, we subsequently only consider the co-rotating case.
- V_{ob} [Fig. 9(b)]: r_{min} is minimised for an obstacle height of $\sim \mu$.
- σ [Fig. 9(c)]: A barrier width $\sigma \sim 2\xi$ best promotes energy driving.
- r_{ob} [Fig. 9(d)]: The barrier position shows a double resonance at 4ξ and 8ξ .

- ϕ_{ob} [Fig. 9(e)]: Maximal energy driving occurs when the vortex and obstacle begin in phase or with the obstacle slightly lagging the vortex.

VI. DISCUSSION

A. Cross-over and induction dynamics

Our precursive study of a single vortex in a double trap revealed cross-over and inductive dynamics. The generation of a vortex state in a neighbouring well of a double-well trap has been studied in [41]. However, there the vortex-containing BEC partially tunnelled into the adjacent empty well, and so is a distinct creation mechanism to the one observed here. While these regimes are interesting in their own right, from the perspective of exploring cross-talk and parametric driving of vortex they pose limitations on the parameter space in which vortices are stable.

B. Cross-talk between vortices

Our main results demonstrate cross-talking between two vortices. When the vortices have the same polarity and different initial positions, they undergo periodic exchanges of energy with each other, transferred via sound waves. We may view this as the driving of a vortex by sound from another vortex. The transfer of energy is rapid: a full energy cycle typically occurs within 10 vortex precessions.

Sound is emitted from each vortex due to its acceleration in the trap. This emitted sound has a quadrupolar radiation pattern and forms an outwardly propagating spiral wave [21] that carries angular momentum of the same orientation as the originating vortex (to conserve angular momentum). Upon passing into the opposing well it imparts some of its energy and angular momentum to the opposing vortex. If the angular momentum carried by the sound waves is of the same orientation as the receiving vortex (which is to say that the vortices are of the same polarity), it serves to increase the angular momentum and energy of this vortex, causing it to move towards the high density trap centre. By the same simple argument, one would expect that when the vortices are of opposite polarity, the energy and angular momentum of the opposing vortex would be reduced. However, no exchange of energy is observed when the vortices have opposing polarity. We will return to this anomaly below. The cross-talk between vortices is analogous to that occurring for dark solitons in the 1D analog of this system [32]. However, where the energy transfer for solitons occurs over many tens of oscillations, the energy transfer for vortices can occur in less than 10 oscillations. Thus the vortex system appears a beneficial platform to experimentally observe and explore these related sound phenomena.

C. Parametric driving of a vortex

By moving a localised Gaussian obstacle through one well, we are able to generate angular-momentum carrying sound waves. When this angular momentum is of the same sign as the vortex, this acts to drive energy into the vortex, but when it of opposite sign it is essentially invisible to the vortex, as seen above for the vortex-vortex transfer. Under constant driving, the vortex energy oscillates periodically and the oscillation amplitude can be resonantly tuned via the obstacle parameters. The driving is most effective when the time-dependent density perturbation created by the obstacle closely matches that of the vortex, i.e. the same width, precession frequency and amplitude. However, the vortex-obstacle energy transfer is considerably slower than vortex-vortex transfer, suggesting that the most “natural” sound to drive a vortex is that from another vortex.

An analogous set-up was studied in [42], except the vortex and obstacle resided in the same trap. There the precessing obstacle periodically formed a vortex at the condensate edge and drove it into the centre. The dynamics were interpreted as nonlinear Rabi cycling from the ground state to the first vortex state. Similarly, we may interpret our observations as oscillations between a high and low energy vortex state. Our results suggest that sound waves may have played a central role in transferring energy from the obstacle to the vortex in [42].

Our findings mirror those relating to driving of dark matter-wave solitons in [18]. There, 1D oscillating paddles were employed to impart linear momentum to the condensate sound field which in turn led to energy being driven into the dark soliton. Resonant driving occurred when the paddles were oscillated at close to the frequency of the undriven soliton motion. Furthermore, when the drive was switched off the soliton maintained that energy (in the absence of phenomenological dissipation), subject to oscillations from the background density excitations.

D. Insight into sound absorption in trapped and homogeneous systems

Using an acoustic ray model, Nazarenko *et al.* [24, 25] find that certain trajectories of sound waves incident on a vortex line can spiral into the vortex core, imparting their energy to the vortical flow. Despite this and our observations herein, sound absorption is not cited to play a significant role in superfluid Helium systems, e.g. quantum turbulence [2, 3].

Consider an infinite homogeneous system containing a tangle of vortex lines. Within this, consider an element of vortex line emitting a pulse of sound due to some acceleration. From the point of emission, the sound spreads out radially. This rapidly dilutes its energy and momentum density, and thus its capacity to influence a line element in its path. Superimpose many such events from many randomly oriented vortex lines and the combined sound

field will be tends towards being isotropic with no net angular momentum. As such it is not surprising that sound absorption is insignificant in these systems.

Now consider our trapped BEC. Sound radiated outwards by an accelerating vortex will eventually reflects off the trap wall and become partially focussed towards the trap centre. While the effectiveness of the focussing will vary with vortex position and trap shape, it will nonetheless lead to a greater and more sustained sonic energy and momentum density than in a homogeneous system, which a suitably placed vortex may be able to gain from. The focussing effect will, however, be shortlived as the sonic angular momentum will become randomised after several reflections in the trap. We see this in Fig. 4 where a large sound pulse with net momentum is rapidly randomised into an isotropic sound field. This further explains the rapid equilibration of the vortex energy when the driving is terminated. These simple arguments suggest that sound absorption may play a significant role in trapped condensates.

Irrespective of the source of the sound, we observe transfer of energy between sound and vortex only when they have the same sign of angular momentum. We may interpret this in terms of the acoustic ray picture [24, 25] which predicts that trajectories of sound spiral into the vortex core and dump their energy and momentum. There the sound was modelled as plane waves while in the BEC the incident sound is a spiral wave carrying angular momentum. The crucial aspect is that, when the sound waves have the same angular momentum as the vortex, they naturally wrap around the vortex, promoting them to spiral into the core. Conversely, when the sound has opposite angular momentum, it will tend to be deflected and repelled by the vortex, unable to impart its angular momentum. In essence, the vortex is invisible to sound waves of opposite angular momentum.

In our quasi-2D system, the vortex line is rectilinear and can only raise its energy by moving to regions of higher density. In 3D system, the vortex can additionally increase its energy by increasing its line length or developing excitations, e.g. Kelvin waves. It is not clear which route to absorb energy would be favoured in 3D, although the orientation of the incoming sound is likely to play a deciding role. In systems of multiple vortices, the position of the vortices provides another route to modify the total vortical energy. Furthermore, symmetric excitations such as vortex rings and vortex-antivortex pairs carry linear momentum and so can be expected to interact predominantly with sound waves of linear momenta, much like dark solitons.

VII. PROPOSED EXPERIMENTAL REALIZATION

A. Set-up details

The double trap used thus far (defined by Eq. (2)) is idealized and not experimentally realizable. Here we will demonstrate that the same qualitative phenomena occur in experimentally-realizable traps. We approximate the idealized double harmonic trap by considering a single elliptical harmonic trap which is split by a central Gaussian barrier. The “split trap” has the form,

$$V(x, y) = \frac{m}{2} \left[\left(\frac{\omega}{2} \right)^2 x^2 + \omega^2 y^2 \right] + V_B e^{-x^2/2d^2} - V_{\min}, \quad (5)$$

where,

$$V_{\min} = -m\omega^2 d^2 \left[\ln \frac{V_B}{m\omega^2 d^2} + 1 \right], \quad (6)$$

is an offset introduced such that the minimum of the potential is zero. The height of the barrier relative to the trap minimum V_0 is related to these parameters via $V_0 = V_B - V_{\min}$. We set the barrier width to be $d = 5\xi$. Figure 10 compares the split trap of Eq. (6) with the idealized double harmonic trap of Eq. (2).

Experimentally, the harmonic trap can be formed via magnetic or optical fields, while the Gaussian barrier is formed by a blue-detuned laser beam aligned along the y -axis. As previously, the system we simulate satisfies $\mu = 10\hbar\omega$. Let us give some typical values for our units. We will assume some typical values: a 2D peak density of $n_0 = 10^{14} \text{m}^{-2}$, an axial trap frequency of $\omega_z = 2\pi \times 1000$ Hz and a radial trap frequency of $\omega_r = 2\pi \times 50$ Hz. Then, for a ^{87}Rb (^{23}Na) condensate, the healing length becomes $\xi = 0.3$ (0.7) μm , the speed of sound $c = 3$ (4) mms^{-1} and the time unit $(\xi/c) = 90$ (175) μs .

B. Cross-talk of two vortices

Each well is no longer circularly symmetric and so the vortex displacement now becomes sensitive to the direc-

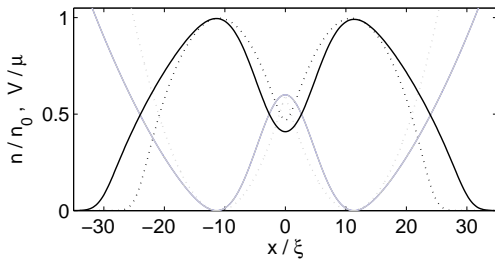


FIG. 10: The experimentally realizable split-trap (grey solid line) and its vortex-free density profile (black solid line) along the y -axis. The analogous potential (grey dashed line) and density (black dashed line) for the double harmonic trap are shown.

tion chosen. As such we will specify the y -displacement of the vortices rather than the radial displacement. Figure 11 shows the phase diagram for one and two vortices in the split trap, as a function of the vortex position y_v and the trap barrier height V_0 . They show close agreement with the corresponding plots for the double harmonic trap, Figs. 2 and 6(a), and demonstrate the same regimes of the vortex dynamics, e.g. cross-over and inductive dynamics.

Choosing a case from the two vortex system (Fig. 11(b)) where the vortex dynamics is stable [$y_v = 3\xi$ and $V_0 = 0.5\mu$], we show the evolution of the vortices in Fig. 12. The vortices clearly drift in and out of the trap centre, out of phase with each other. This corresponds to the same transfer of energy observed in the idealized trap in Fig. 7(a). The period of the energy transfer is around $1600(\xi/c)$ which is around 8 vortex precessions. Snapshots of the condensate density show the initial appearance of the condensate (vortex 1 at large radius and vortex 2 at the trap centre), after a half-cycle of energy exchange (vortex 1 at the trap centre and vortex 2 at large radius) and after a full cycle of energy exchange (vortex 1 returns to large radius and vortex 2 returns to the trap centre).

C. Precessing obstacle

We now turn to the system with one vortex and a precessing obstacle. The addition of a precessing Gaussian obstacle to a harmonic trap has been demonstrated experimentally [9, 38]. The obstacle parameters we employ are obstacle width $\sigma = 2\xi$, obstacle amplitude $A_{\text{ob}} = \mu$, $y_{\text{ob}} = 3\xi$, $\phi_{\text{ob}} = 0$ and $\omega_{\text{ob}} = 0.234\omega$. The ensuing dynamics of the vortex is shown in Fig. 13. The vortex gradually spirals into the trap centre, indicating the

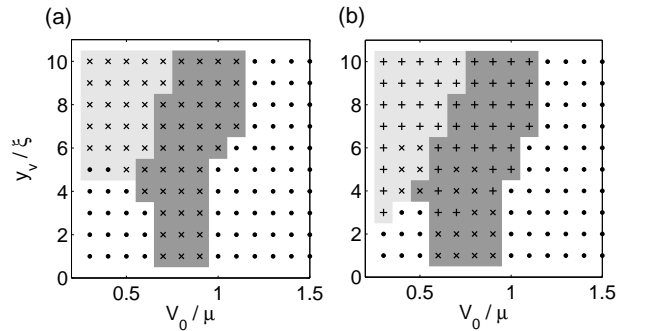


FIG. 11: Phase diagrams for vortex dynamics in the split trap as a function of vortex displacement y_v and barrier height V_0 . (a) A single vortex in the right-hand well, displaced by y_v from the well centre. Dots (crosses) correspond to the final state [after $5000(\xi/c)$] being a vortex (vortex-free) state. (b) A vortex in each well, of the same polarity. The final state is either two vortices (dots), one vortex (pluses) or no vortices (crosses). In (a) and (b) the light-shaded (dark-shaded) region corresponds to case I (II) of vortex dynamics.

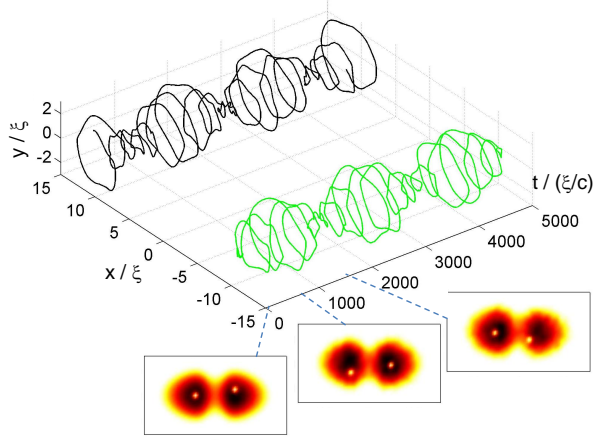


FIG. 12: Vortex motion during cross-talk in the experimental split trap. Also shown are plots of the condensate density at times $t = 0, 850$ and 1550 (ξ/c). The vortices move anti-clockwise with respect to these density profiles. The color-density mapping is defined as black/white=high/zero density. Parameters: $V_0 = 0.5\mu$ and $y_v = 3\xi$.

steadily increase in its energy and angular momentum. As in the double harmonic trap, the vortex-obstacle energy transfer is slower than the vortex-vortex case, with minimal position/maximal energy reached after $\sim 10^4(\xi/c)$. Note that the split trap system demonstrates the same resonant behaviour as in Fig. 9, for example, there is a sharp resonance in the obstacle precession frequency which closely coincides with the precession frequency of the unperturbed vortex ($\sim 0.234\omega$).

D. Experimental observation

The vortex-vortex and vortex-obstacle energy transfer could be observed through the evolution of the vortex position as it spirals in and out of the trap. Real-time tracking of vortices was recently demonstrated [13]. In brief this involves transferring (via pulsed microwave radiation) a small proportion of the BEC into an untrapped state, allowing this representative cloud to expand such that the vortex cores become optically resolvable, and performing absorption imaging of the cloud. By repeating this at time intervals, the vortex motion can be tracked. For ^{87}Rb (^{23}Na) the period of the energy exchange for the vortex-vortex case presented here is ~ 0.15 (0.3)s, while for the vortex-obstacle case it is ~ 1.8 (3.5)s. These timescales are well within the experimental lifetime of vortices in BECs, which can be as large as 10 s [7].

VIII. CONCLUSION

We have shown that two vortices in a double trap can undergo a coherent cross-talk, periodically exchange-

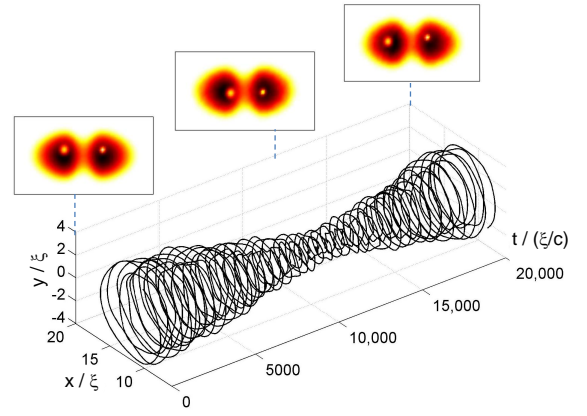


FIG. 13: Vortex motion under parametric driving by a precessing obstacle in the experimental split trap system. The condensate density is presented at times $t = 0, 12000$ and 20000 (ξ/c). In the density plots, the hole in the left-hand well corresponds to the obstacle and the hole in the right-hand well to the vortex, and both move anti-clockwise. Parameters: $y_v(t=0) = 3\xi$, $V_0 = 0.5\mu$, $\sigma = 2\xi$, $A_{ob} = \mu$, $y_{ob} = 3\xi$ and $\omega_{ob} = 0.234\omega$.

ing energy and angular momentum over long-range via sound waves. These observations are strongly analogous to the interaction of dark solitons mediated by linear-momentum-carrying sound waves. This adds further evidence for the striking acoustic similarities of vortices and dark solitons, despite no mathematically rigorous link. Sound waves artificially generated by a moving obstacle are similarly found to drive energy into a vortex. Crucially, for the sound to be absorbed by the vortex, it must carry angular momentum of the same sign as the vortex; if the sound has opposite angular momentum it is essentially invisible to the vortex.

Our observations are robust: we have confirmed that we observe the same qualitative dynamics for different condensate parameters (e.g. a large, more Thomas-Fermi condensate) and double trap parameters. Importantly, our observations occur in experimentally realizable double well geometries, and within both the timescales of current vortex experiments and the timescale of other dissipation mechanisms, e.g. thermal dissipation [43, 44]. Our prediction of parametric driving of a vortex using a precessing obstacle could be used to counteract thermal dissipation of vortices, as suggested for dark solitons [18].

Trapping appears to promote sound absorption, suggesting that this may play a much greater role in trapped BECs than in homogeneous superfluids. An example may lie in the formation of vortex lattices in rotating atomic BECs. The nucleated vortices are observed experimentally to crystallize into a vortex lattice, a process that requires dissipation. While this is provided by thermal dissipation at raised temperatures [45–47], experimental and theoretical observations at very low/zero temperature suggest that crystallization is temperature-independent [48–51]. Vortex-sound interactions may pro-

vide such a mechanism.

Establishing the rudimentary interactions between vortices and sound in quantum fluids will aid in exploring and understanding more complex scenarios, such as those present in large-scale quantum turbulence [3] and analogs of black hole superradiance based on scattering of sound

waves from superfluid vortices [52, 53]. In future work we hope to explore sound absorption in 3D vortex lines and pursue acoustic ray models of sound absorption in trapped condensates.

We acknowledge funding from the EPSRC.

-
- [1] R. J. Donnelly *Quantized Vortices in Helium II* (Cambridge University Press, Cambridge, 1991).
 - [2] C. F. Barenghi, R. J. Donnelly, and W. F. Vinen, eds., *Quantized vortex dynamics and superfluid turbulence* (Springer, Berlin, 2001).
 - [3] W. F. Vinen, *J. Low Temp Phys.*, **161**, 419 (2010).
 - [4] A. L. Fetter and A. A. Svidzinsky, *J. Phys.: Cond. Matt.* **13**, R135 (2001).
 - [5] B. P. Anderson, *J. Low Temp. Phys.* **161**, 574 (2010).
 - [6] M. R. Matthews, B. P. Anderson, P. C. Haljan, D. S. Hall, C. E. Wieman, and E. A. Cornell, *Phys. Rev. Lett.* **83**, (1999).
 - [7] P. Rosenbusch, V. Bretin, and J. Dalibard, *Phys. Rev. Lett.* **89**, 200403 (2002).
 - [8] P. Engels, I. Coddington, P. C. Haljan, V. Schweikhard, and E. A. Cornell, *Phys. Rev. Lett.* **90**, 170405 (2003).
 - [9] T. W. Neely, E. C. Samson, A. S. Bradley, M. J. Davis, and B. P. Anderson, *Phys. Rev. Lett.* **104**, 160401 (2010).
 - [10] N. S. Ginsberg, J. Brand, and L. V. Hau, *Phys. Rev. Lett.* **94**, 040403 (2005).
 - [11] E. A. L. Henn, J. A. Seman, G. Roati, K. M. F. Magalhães, and V. S. Bagnato, *Phys. Rev. Lett.* **103**, 045301 (2009).
 - [12] G. P. Bewley, D. P. Lathrop and K. R. Sreenivasan, *Nature* **441**, 588 (2006).
 - [13] D. V. Freilich, D. M. Bianchi, A. M. Kaufman, T. K. Langin and D. S. Hall, *Science* **3**, 1182-1185 (2010).
 - [14] O. Bühler, *Ann. Rev. Fluid Mech.* **42**, 205 (2010).
 - [15] M. Leadbeater, T. Winiecki, D. C. Samuels, C. F. Barenghi and C. S. Adams, *Phys. Rev. Lett.* **86**, 1410 (2001).
 - [16] E. Lundh and P. Ao, *Phys. Rev. A* **61**, 063612 (2000).
 - [17] W. F. Vinen, *Phys. Rev. B* **64**, 134520 (2001).
 - [18] N. P. Proukakis, N. G. Parker, C. F. Barenghi and C. S. Adams, *Phys. Rev. Lett.* **93**, 130408 (2004).
 - [19] C. F. Barenghi, N. Parker, N. Proukakis, and C. Adams, *J. Low Temp. Phys.* **138**, 629 (2005).
 - [20] M. Leadbeater, D. C. Samuels, C. F. Barenghi, and C. S. Adams, *Phys. Rev. A* **67**, 015601 (2003).
 - [21] N. G. Parker, N. P. Proukakis, C. F. Barenghi, and C. S. Adams, *Phys. Rev. Lett.* **92**, 160403 (2004).
 - [22] S. I. Davis, P. C. Hendry, and P. V. E. McClintock, *Physica B - Cond. Matt.* **280**, 43 (2000).
 - [23] P. M. Walmsley, A. I. Golov, H. E. Hall, A. A. Levchenko, and W. F. Vinen, *Phys. Rev. Lett.* **99**, 265302 (2007).
 - [24] S. V. Nazarenko, *Phys. Rev. Lett.* **73**, 1793 (1994).
 - [25] S. V. Nazarenko, N. J. Zabusky, and T. Scheidegger, *Phys. Fluids* **7**, 2407 (1995).
 - [26] K. W. Schwarz and C. W. Smith, *Phys. Lett. A* **82**, 251 (1981).
 - [27] N. G. Berloff and C. F. Barenghi, *Phys. Rev. Lett.* **93**, 090401 (2004).
 - [28] P. G. Kevrekidis, R. Carretero-Gonzalez, G. Theocharis, D. J. Frantzeskakis and B. A. Malomed, *J. Phys. B* **36**, 3467-3476 (2003).
 - [29] Th. Busch and J. R. Anglin, *Phys. Rev. Lett.* **84**, 2298 (2000).
 - [30] N. G. Parker, N. P. Proukakis and C. S. Adams, *Phys. Rev. A* **81**, 033606 (2010).
 - [31] N. G. Parker, N. P. Proukakis, M. Leadbeater, and C. S. Adams, *Phys. Rev. Lett.* **90**, 220401 (2003).
 - [32] A. J. Allen, D. P. Jackson, C. F. Barenghi, and N. P. Proukakis, *Phys. Rev. A* **83**, 013613 (2011).
 - [33] C. J. Pethick and H. Smith, *Bose-Einstein Condensation in Dilute Gases* (University Press, Cambridge, 2002).
 - [34] A. Minguzzi, S. Succi, F. Toschi, M. P. Tosi, and P. Vignolo, *Phys. Rep.* **395**, 223 (2004).
 - [35] D. S. Rokhsar, *Phys. Rev. Lett.* **79**, 2164 (1997).
 - [36] N. G. Parker, N. P. Proukakis, C. F. Barenghi, and C. S. Adams, *J. Phys. B* **37**, S175 (2004).
 - [37] A. A. Svidzinsky and A. L. Fetter, *Phys. Rev. A* **62**, 063617 (2000).
 - [38] C. Raman, J. R. Abo-Shaeer, J. M. Vogels, K. Xu, and W. Ketterle, *Phys. Rev. Lett.* **87**, 210402 (2001).
 - [39] B. Jackson, J. F. McCann and C. S. Adams, *Phys. Rev. A* **61**, 051603(R) (2000).
 - [40] R. Onofrio, C. Raman, J. M. Vogels, J. R. Abo-Shaeer, A. P. Chikkatur, and W. Ketterle, *Phys. Rev. Lett.* **85**, 2228 (2000).
 - [41] J. R. Salgueiro, M. Zacarés, H. Michinel, and A. Ferrando, *Phys. Rev. A* **79**, 033625 (2009).
 - [42] B. M. Caradoc-Davies, R. J. Ballagh, and K. Burnett, *Phys. Rev. Lett.* **83**, 895 (1999).
 - [43] P. O. Fedichev and G. V. Shlyapnikov, *Phys. Rev. A* **60**, R1779 (1999).
 - [44] B. Jackson, N. P. Proukakis, C. F. Barenghi and E. Zaremba, *Phys. Rev. A* **79**, 053615 (2009).
 - [45] C. Lobo, A. Sinatra, and Y. Castin, *Phys. Rev. Lett.* **92**, 020403 (2004).
 - [46] A. A. Penckwitt, R. J. Ballagh, and C. W. Gardiner, *Phys. Rev. Lett.* **89**, 260402 (2002).
 - [47] M. Tsubota, K. Kasamatsu, and M. Ueda, *Phys. Rev. A* **65**, 023603 (2002).
 - [48] E. Hodby, G. Hechenblaikner, S. A. Hopkins, O. M. Marag, and C. J. Foot, *Phys. Rev. Lett.* **88**, 010405 (2001).
 - [49] J. R. Abo-Shaeer, C. Raman, and W. Ketterle, *Phys. Rev. Lett.* **88**, 070409 (2002).
 - [50] N. G. Parker and C. S. Adams, *Phys. Rev. Lett.* **95**, 145301 (2005).
 - [51] N. G. Parker and C. S. Adams, *J. Phys. B* **39**, 43 (2006).
 - [52] T. R. Slatyer and C. M. Savage, *Class. Quant. Grav.* **22**, 3833 (2005).
 - [53] F. Federici, C. Cherubini, S. Succi, and M. P. Tosi, *Phys. Rev. A* **73**, 033604 (2006).